Preparation of Manganese Oxide–Polyethylene Oxide Hybrid Nanofibers Through *In Situ* Electrospinning

Mohammad Madani,[1] Naser Sharifi-Sanjani,[1] Sepideh Khoee,[1] Ahmad Hasan-Kaviar,[1] Abbass Kazemi[2]

[1]*School of Chemistry, University College of Science, University of Tehran, Tehran, Iran*
[2]*Division of Polymer Science and Technology, Research Institute of Petroleum Industry, Tehran, Iran*

Received 30 May 2009; accepted 15 December 2009
DOI 10.1002/app.31990
Published online 2 March 2010 in Wiley InterScience (www.interscience.wiley.com).

ABSTRACT: Manganese oxide nanoparticles–polyethylene oxide nanofibers as organic–inorganic hybrid were prepared via *in situ* electrospinning. Thus, electrospinning of polyethylene oxide solution with different manganese chloride concentration was carried out in gaseous ammonia atmosphere containing oxygen. The reaction of manganese chloride with ammonia produces manganese hydroxide, and then oxygen in the reaction media reacts with manganese hydroxide to yield manganese oxide. These two reactions occur during fiber formation. Transmission electron microscopy and scanning electron microscopy showed that manganese oxide (MnO_2) nanoparticles were formed on the produced nanofibers of 100–600 nm in diameter. The existence of the formed MnO_2 was also proved by X-ray diffraction analysis, and it showed that the λ-MnO_2 nanoparticles were produced. Differential scanning calorimetry (DSC) analysis was used to determine the melting point and to calculate the crystallinity of the produced hybrid nanofibers. The DSC and thermogravimetric analysis results of the obtained nanofibers were compared with those of the nanofibers produced in electrospinning of pure polyethylene oxide solution. © 2010 Wiley Periodicals, Inc. J Appl Polym Sci 117: 243–249, 2010

Key words: *in situ* electrospinning; polyethylene oxide; manganese oxides nanoparticles

INTRODUCTION

Manganese oxides have long been known as materials of technological importance for electrochemical applications,[1] electrode materials for electrochemical energy storage systems such as cathode materials in alkaline cells,[2] intercalation hosts for lithium batteries,[3,4] and electrode materials in supercapacitors,[1,5] because of their excellent electrochemical performance, low cost, nonpoisonous nature, environmental friendliness, and convenient preparation.[6–8] Furthermore, it can be used in the photovoltaic devices.[9,10]

Polymer nanocomposites containing metal oxides have attracted a great deal of interest from researchers because they frequently exhibit unexpected hybrid properties, synergically derived from both components.[11] Enhanced conductivity and special mechanical, electrochemical, optical, magnetic as well as thermal properties of these composites make them promising materials.

In the past decade, electrospinning has attracted tremendous interests in the research community simply because it provides a facile and effective means in producing ultrafine fibers with diameters ranging from microns down to a few nanometers. Moreover, this procedure can produce functional nanofibers having optical, electrical, or catalytic properties by incorporating inorganic nanoparticles into the nanofibers. Most of the reported manufacturing methods of polymer–inorganic composite nanofibers are based on electrospinning of polymer solution blended with inorganic nanoparticles.[12,13] Another way of preparing polymeric–inorganic composite nanofibers is based on electrospinning of a polymer precursor having metal ions and subsequently post-treating of the produced nanofibers.[14]

The aim of this work is to manufacture organic–inorganic nanofiber hybrids based on a new method through *in situ* electrospinning and is also to show the possibility of these two reactions occurring on the traveling polymer jet in electrospinning with an active atmosphere. Thus, we are reporting *in situ* synthesis of manganese oxide nanoparticles on polyethylene oxide (PEO) nanofibers through electrospinning. Extensive characterization of nanofibers was carried out using transmission electron microscopy (TEM), scanning electron microscopy (SEM), X-ray diffraction (XRD), differential scanning calorimetery (DSC), and thermogravimetric analysis (TGA) techniques, and the results were compared with those of the nanofibers produced in electrospinning of pure PEO solution.

Correspondence to: M. Madani (mmadani@khayam.ut.ac.ir).

TABLE I
Recipes for the Electrospinning Methods

Exp.	$MnCl_2 \cdot 4H_2O$ (g)	Mn^{+2} ions percentage within solution base on PEO (%)	PEO (g)	Atmosphere
M1	0.5	3.5	4	NH_3 and air
M2	1	7	4	NH_3 and air
M3	2	14	4	NH_3 and air
M4	3	21	4	NH_3 and air
M5	4	28	4	NH_3 and air
P	0	0	4	Air
Q	0.5	3.5	4	Air

EXPERIMENTAL

$MnCl_2 \cdot 4H_2O$ (supplied by Merck Chemical, Germany) with different concentrations (given in Table I) was dissolved in 100 mL distilled water to produced manganese chloride $MnCl_2$ solution. Then, the following seven experiments [Exp. M1, M2, M3, M4, M5 (collectively called M-series in this article), P, and Q] were carried out. M-series: 4.0 g of polyethylene oxide (PEO with weight average molecular weight of 600,000 g/mol and supplied by Acros Organics, Belgium) was added to 100 mL of earlier-mentioned manganese chloride solution with different concentrations (given in Table I) and left for two nights to obtain a homogenous PEO solution having manganese chloride. The polymer solution was put into a hypodermic syringe. A syringe pump (Stoelting, USA) was used to feed the polymer solution into a metallic needle with an inner diameter of 0.7 mm. A grounded aluminum foil as collector was placed at a fixed distance of 18 cm from the needle. The metallic needle and the collector were enclosed in a polymethyl metacrylate box (40 cm × 50 cm × 60 cm). The feed rate of the syringe pump was fixed at 0.7 mL/h. A positive potential of 18 kV was then applied to the polymer solution using a high-voltage power supplier (MH 100 series, HiTek Power, UK) with a maximum voltage of 50 kV. During electrospinning, gaseous ammonia (from a cylinder purchased from Merck Chemical) was purged into the box with a rate of 10 L/min. Electrospun nanofibers were collected on the surface of the grounded aluminum foil.

For comparison, the electrospinning of the aforementioned PEO solution having manganese ions (Exp. Q) and a pure PEO solution in an air atmosphere (Exp. P) was also carried out in a way similar to M-series.

A CEM 902A ZEISS Transmission Electron Microscope (TEM) with an accelerating voltage of 80 kV

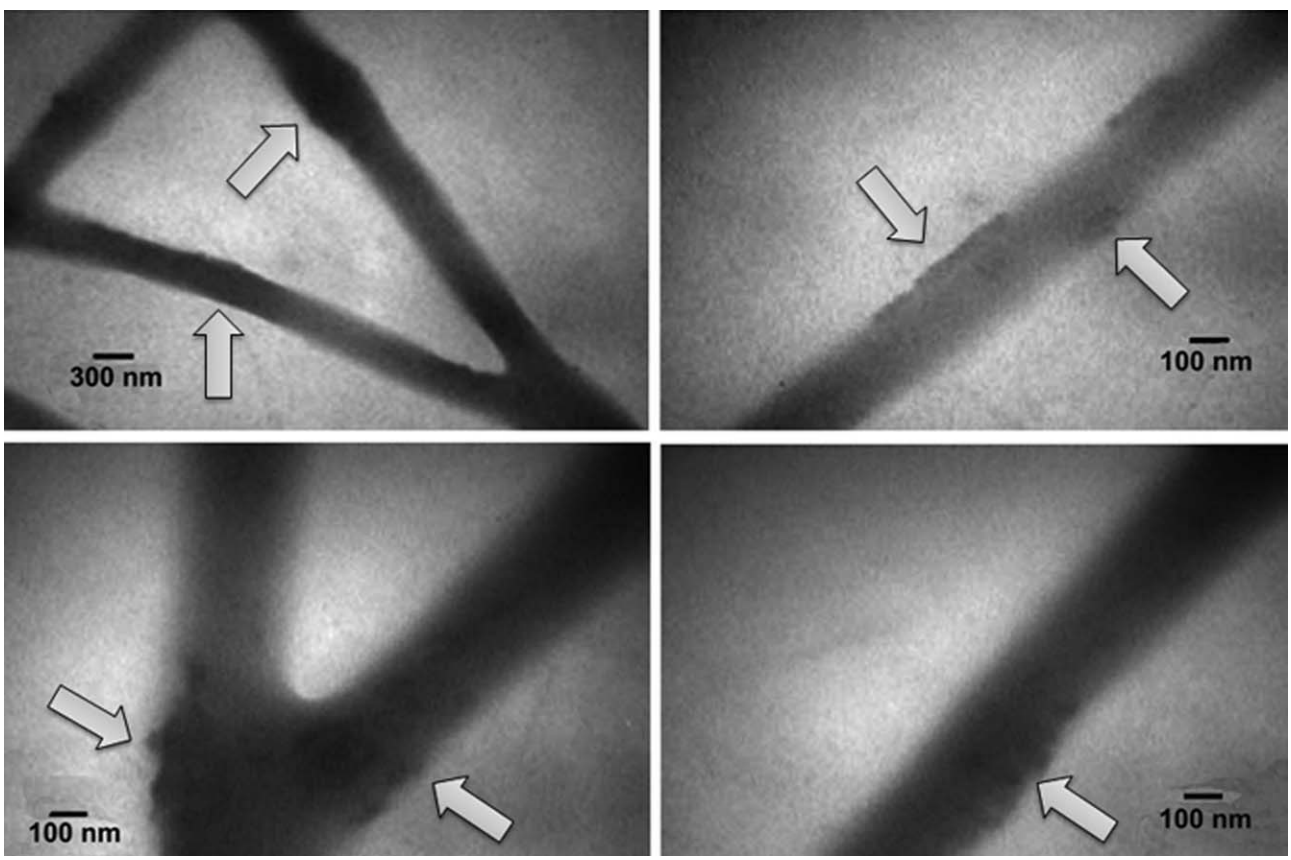

Figure 1 TEM images of nanofibers obtained from Exp. M1 (the manganese oxide was pointed out).

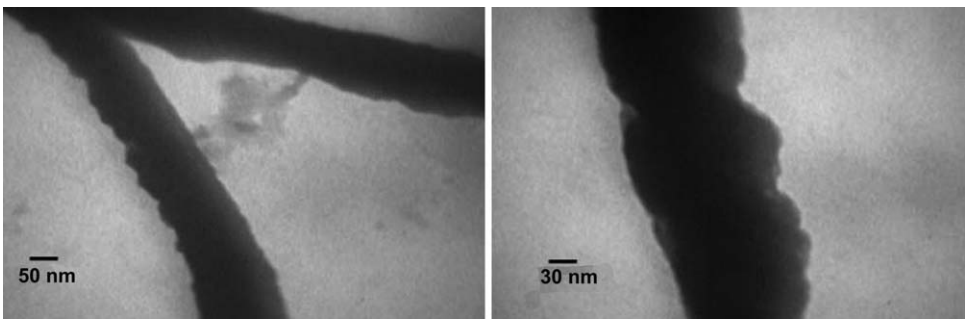

Figure 2 TEM images of nanofibers obtained from Exp. M4.

was used to obtain more information about the morphology of fibers and to confirm the presence of MnO_2 nanoparticles. The electrospun fibers were directly deposited onto a copper grid and then analyzed by TEM technique. The size and morphology of nanofibers were investigated by SEM with a ZEISS DSM 960A instrument. For SEM analysis, the nanofibers were coated with gold.

Thermal properties of the electrospun fibers were analyzed by thermogravimetry (Model TGAQ50, TA Instruments) for heating rate at 20°C/min and DSC (Model DSCQ100, TA Instruments) for heating rate at 10°C/min under the inert gas of Ar.

XRD patterns of the samples were recorded by an Expert Philips diffractometer with a CuKα anode; scans were made from 10° to 100° (2θ). The nanofiber mats were deposited on a glass during electrospinning and then analyzed by XRD method. FTIR spectra were obtained using a Bruker Equinox 55 spectrophotometer.

RESULTS AND DISCUSSION

A light-brown fiber mat was obtained in M-series, whereas a white fiber mat was obtained in P experiment. A comparison of the appearance of the mats obtained from M-series with that of the P fiber mat suggested that the manganese ions in the jet traveling in the distance between the needle and the collector could precipitate in the gaseous ammonia atmosphere to produce manganese hydroxide and then alkaline oxidation reaction of manganese hydroxide with oxygen present in the box during fibers formation produces MnO_2.[15] In other words, in this process two reactions occur during fibers formation: first, the reaction of Mn^{+2} ions with NH_3, which produces $Mn(OH)_2$, and second, the reaction of $Mn(OH)_2$ with oxygen, which produces MnO_2 nanoparticles.

Figure 1 displays the TEM images of fibers obtained from Exp. M1 (electrospinning of PEO solution having 3.5% Mn^{+2} based on PEO, in ammonia and oxygen atmosphere) and as it shows, dark spots of MnO_2 are heterogeneously dispersed on the fibers as a shell. Figure 2 presents the TEM images of fibers produced in Exp. M4 (electrospinning of PEO solution having 21% Mn^{+2} based on PEO, in ammonia and oxygen atmosphere). Both images, Figures 1 and 2, suggest that in the Exp. M1, MnO_2 nanoparticles were heterogeneously synthesized on fibers through the reaction of manganese ions with NH_3 and oxygen, and in Exp. M4, a greater number of MnO_2 nanoparticles are formed on the nanofibers through *in situ* chemical reactions during electrospinning and the contrast of two phases (MnO_2 and PEO) was eliminated because of the higher concentration of the MnO_2 within M4 fibers than in M1 fibers. In Exp. M1, MnO_2 particles aggregate to form nanoparticles on the fibers probably because of the insignificant interaction of MnO_2 with PEO. This causes MnO_2 nanoparticles in Exp. M1 to randomly form on the fibers in a larger size and a lesser number than MnO_2 nanoparticles formed in Exp. M4. TEM images of P nanofibers did not show these events (Fig. 3).

Figure 4 displays SEM images of all produced fibers. It can be concluded from these images that by increasing the inorganic portion within the fibers, the morphology of the fibers change, and SEM image of M5 fibers [Fig. 4(e)] shows an especial morphology that is not similar to the other ones because of the large amount of MnO_2 within the fibers. The diameter of the M1, M2, M3, M4, and M5 fibers are within the range of 150–300, 120–250, 120–300, 100–150, and 120–600 nm, respectively, based on SEM images.

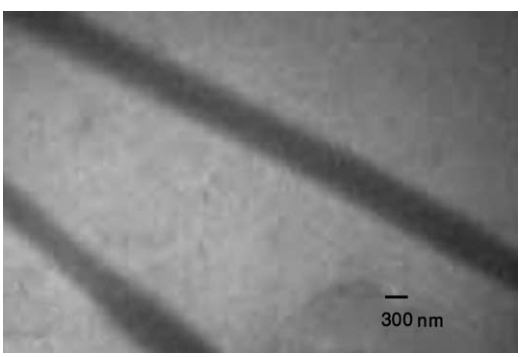

Figure 3 TEM image of nanofibers obtained from Exp. P.

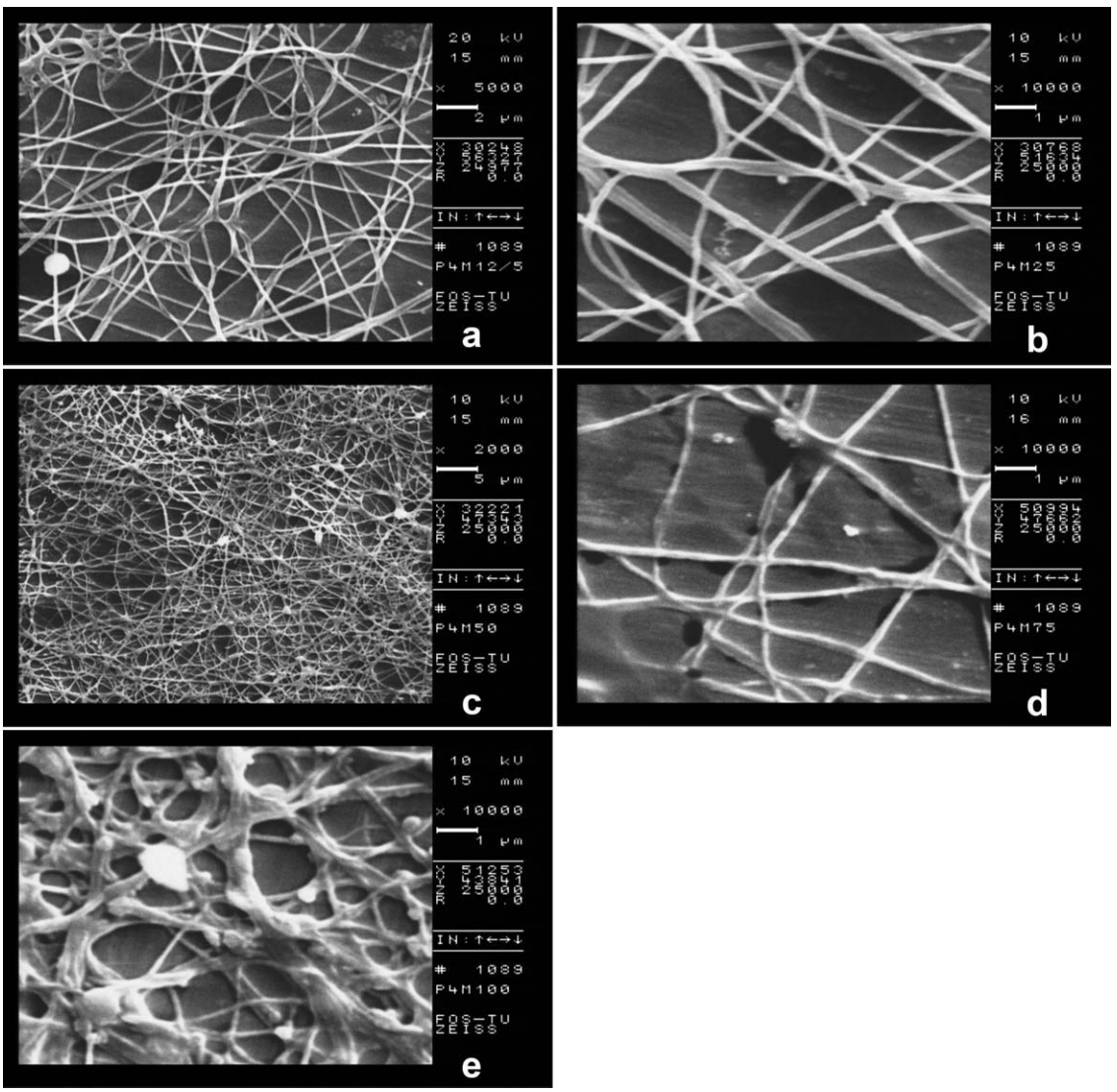

Figure 4 SEM images of nanofibers obtained from experiments M1 (a), M2 (b), M3(c), M4 (d), and M5 (e).

The TGA and DTGA thermograms for the pure PEO fibers and their nanocomposites with different weight percentage of MnO_2 are given in Figure 5. The curves a, b, c, d, and e in Figure 5 are TGA thermographs of fiber mats obtained in Exp. M5, M4, M3, M1, and P, respectively. The initial degradation

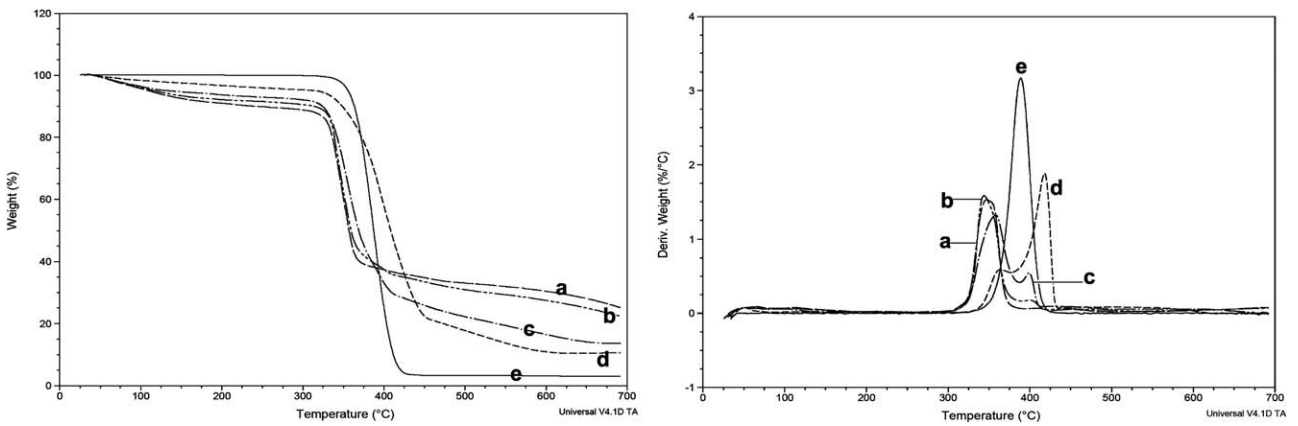

Figure 5 TGA and DTGA thermographs of M1 (d), M3 (c), M4 (b), M5 (a), and P (e) fibers.

TABLE II
Thermal Decomposition Temperatures and Residue of the Products Obtained from the TGA Analyses

Sample	T_{onset} (°C)	T_d (°C)	Losing weight between 100–150°C (%)	Residue at 680°C (%)
M1	319	417	0.687	12.36
M3	308	358	1.52	17.25
M4	313	344	2.29	26.78
M5	311	347	2.68	29.92
P	330	388	0.02	2.90

temperature (T_{onset}) and the thermal decomposition temperature (T_d, obtained by the first derivative of TGA curves) for pure PEO fibers and their composite fibers are summarized in Table II.

The pure PEO degrades in nearly one step around 320–420°C. The comparison of curves a–d with curve e shows that the presence of MnO_2 nanoparticles in fibers (as shown in curves a and b) reduce the thermal properties of PEO fibers. The T_d of the composites decrease as compared with the pure PEO as the amount of MnO_2 increases in the matrix, but because of some factors, such as aggregation of MnO_2 nanoparticles, there is no linear relationship between MnO_2 amounts within the fibers and T_d of composite fibers.

By comparison of residue at 680°C (Table II), the increase in residue by the increase in MnO_2 concentration within the fibers can be concluded, and the percentage of the MnO_2 within the fibers can be calculated.

The release of loosely bonded water between 100 and 150°C in composite fiber corresponds to an endothermic process. The weight loss of M4 fibers is higher in this region in comparison with other ones because of larger amounts of $MnO_2{\cdot}xH_2O$ within M4 fibers than other ones.

Thermal properties of the fiber mats produced in the experiments (Exp. M1, M3, M4, and M5) were also analyzed by DSC analysis. The DSC thermographs of the experiments are given in Figure 6, and the curves a, b, c, and d in this figure are DSC thermographs of fiber mats obtained in Exp. M5, M4, M3, and M1, respectively. The melting points (T_m), crystallization temperature (T_C), and the percentage of crystallinity (X_C %) of the products in the experiments were obtained from the DSC analyses and are listed in Table III.

The presence of an intense melting peak in the DSC thermographs indicates the semicrystalline products. This figure shows that the melting point of the M-series fibers in curves a–d is lower than P fibers.

The specific heat of crystallization of the nanocomposite ΔH_{comp} was calculated using the following formula:

$$\Delta H_{comp} = [\Delta H_{total} \times 100]/y$$

where ΔH_{total} is obtained from the peak area of the DSC curve (J/g), and y is the concentration of PEO (wt %). The given crystallinities (X_C %) of the fiber mats in Table III were calculated using the equation $X_C\ \% = [\Delta H_{comp}/\Delta H_f^o] \times 100$, where ΔH_f^o is the heat of fusion of completely crystalline PEO (that is 213.7 J/g)[16], and ΔH_{comp} is the heat of fusion for the sample calculated from the former equation. As shown in Figure 6 and Table III, the melting point and the crystallinity of pure PEO fibers (Exp. P) are higher than those of PEO fibers having MnO_2 nanoparticles within them.

The data given in Table III also show that the crystallinity and melting point of the fibers produced in Exp. P are higher than those in M-series. This is a result of the presence of MnO_2 nanoparticles in fibers produced in M-series.

The fiber mats obtained from the Exp. P, Q, and M1 were also analyzed by XRD analysis of which the patterns are given in Figure 7. An initial conclusion could be that the patterns in this figure are different. The two strong peaks appearing at 2θ of

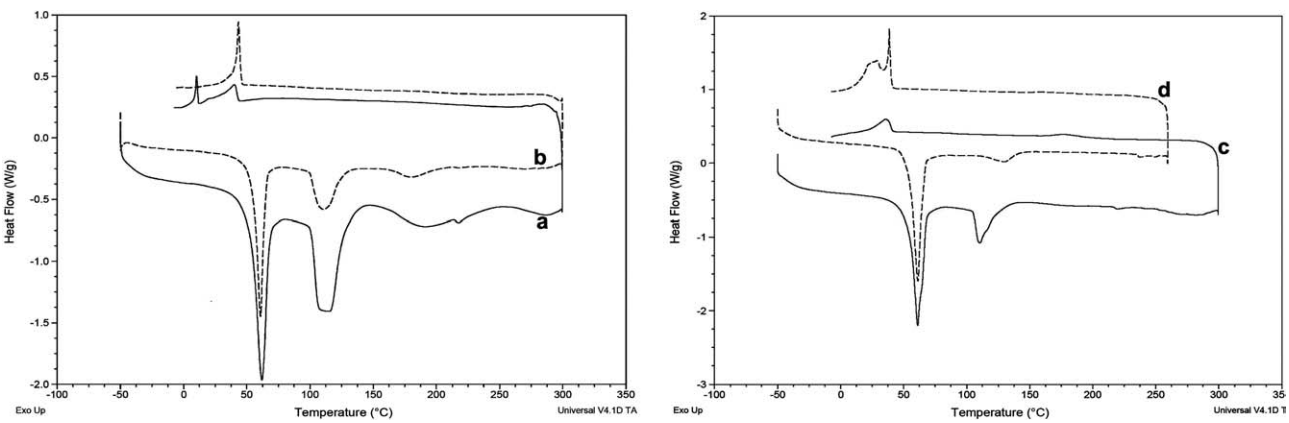

Figure 6 DSC thermographs of M5 (a), M4 (b), M3 (c), and M1 (d) fibers.

TABLE III
The Melting Points (T_m), Crystallization Temperature (T_C), and the Percentage of Crystallinity (X_C %) of the Products Obtained from the DSC Analyses

Sample	Heating T_m (°C)	Enthalpy of fusion ΔH_{total} (J/g)	Cooling T_c (°C)	Enthalpy of crystallization (ΔH) (J/g)	Crystallinity (%)
M1	54.0	83.7	39.8	53.4	41.5
M3	54.7	101.0	40.9	17.4	33.2
M4	55.2	52.6	45.5	15.2	38.8
M5	53.5	85.8	11.7	16.2	46
P	59.1	128.8	–	–	60

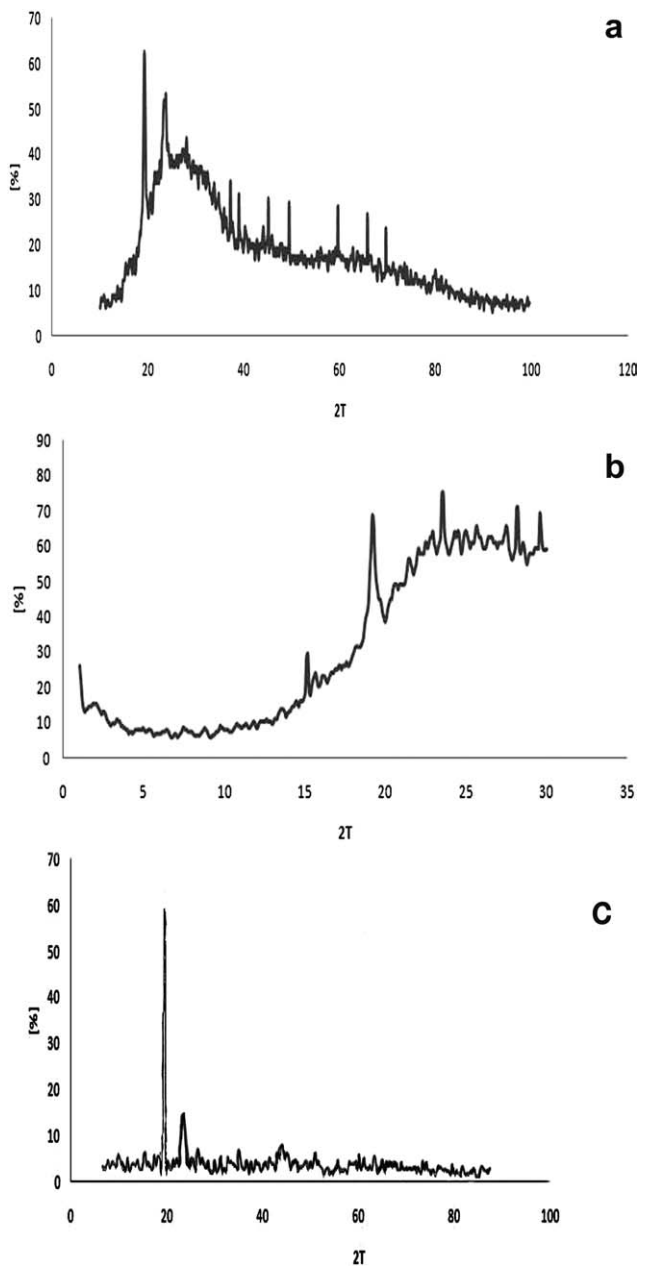

Figure 7 XRD patterns of the nanofiber mats produced in the experiments: M1 (a), Q (b), and P (c).

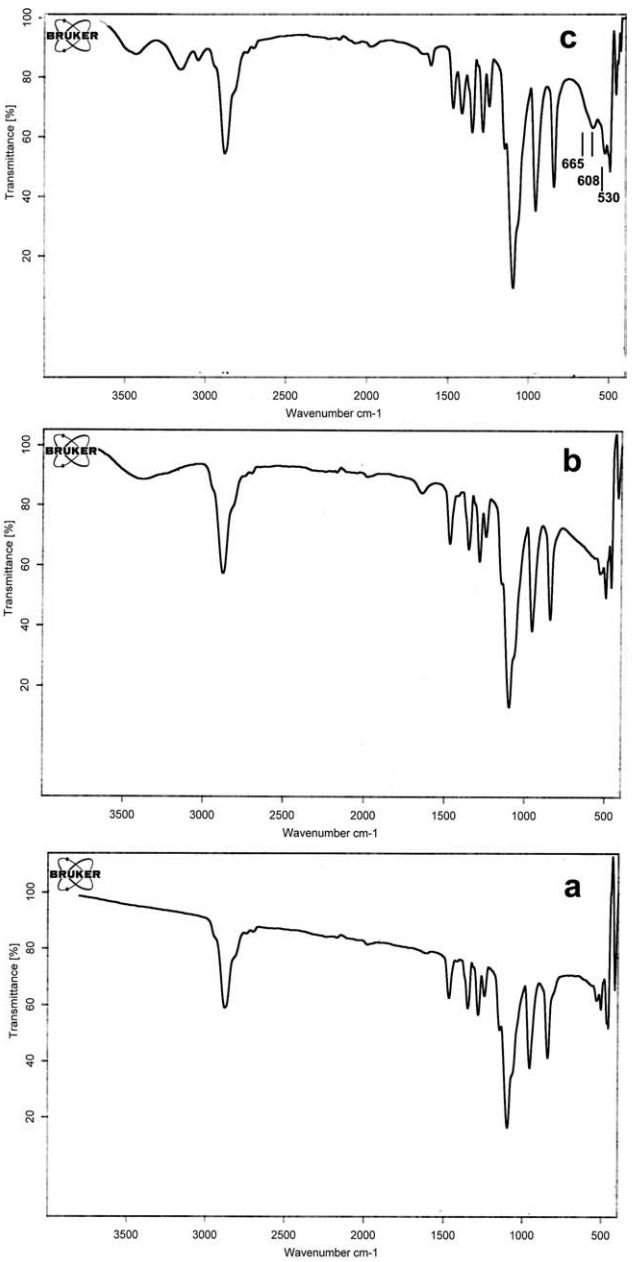

Figure 8 FTIR spectra of P fibers (a), Q fibers (b), and M1 fibers (c).

$\sim 19^\circ$ and 23° in Figure 7 are assigned to crystalline PEO.[17] The XRD pattern of the M1 fibers [Fig. 7(a)] also displays some peaks at 2θ values of 19.1°, 37.1°, 38.9°, 45.0°, 49.5°, 59.6°, 65.7°, and 69.6°, which are related to manganese oxide (λ-MnO_2). These peaks are not present in Figure 7(b) (the product obtained in the electrospinning of a PEO solution having manganese ions in an air atmosphere, i.e., Q experiment) and Figure 7(c) (the product obtained in the electrospinning of pure PEO solution, i.e., P experiment).

The FTIR spectra of P fibers (a), Q fibers (b), and M1 fibers (c) are shown in Figure 8. The crystalline PEO exhibits the vibration (COC) mode as a triplet at 1148, 1110, and 1062 cm^{-1} with a maximum at 1110 cm^{-1},[18] and MnO_2 gave double degenerate vibrations at 665–678 cm^{-1} (this double degenerate peak of MnO_2 appeared at 665 cm^{-1} as shoulder peak for the M1 composite fibers) and strong peaks at 530 and 608 cm^{-1}.[19] The mentioned peaks were all found in the FTIR spectrum of the resulting M1 composite fibers. It confirms the formation of MnO_2/PEO composite fibers.

All of the results obtained by the earlier-mentioned analyses elucidate the ability of reaction of traveling polymer jet in electrospinning with an active atmosphere, and this procedure has potential implications in easy production of organic–inorganic hybrid nanofibers and nanostructures.

CONCLUSIONS

Inorganic–polymeric hybrid nanofibers were produced through electrospinning. The nanofibers with 100–600 nm in diameter were produced via occurrence of two reactions (first, the reaction of Mn^{+2} ions with NH_3, which produces $Mn(OH)_2$, and second, the reaction of $Mn(OH)_2$ with oxygen, which produces MnO_2) during electrospinning of PEO solution having $MnCl_2$ in ammonia and oxygen atmosphere. The amounts of MnO_2 within the fibers decrease with the decreases in the $MnCl_2$ concentration in starting solution. The crystallinity of PEO, shown by DSC analyses, was reduced in electrospinning process in the presence of MnO_2 nanoparticles at high concentration.

The authors thank Mr. Hashemi for providing TEM and SEM micrographs from the Laboratory of Electronic Microscopy of University College of Science in the University of Tehran. They also thank Ms. Fotouhi. Great gratitude is expressed towards the financial support of the Vice-Presidency for Science and Technology and the University of Tehran.

References

1. Lee, H. Y.; Goodenough, G. B. J Solid State Chem 1999, 144, 220.
2. Chabre, Y.; Pannetier, J. Prog Solid State Chem 1995, 23, 1.
3. Thackeray, M. M. Prog Solid State Chem 1997, 25, 1.
4. Rossouw, M. H.; Liles, D. C.; Thackeray, M. M. Mater Res Bull 1992, 27, 221.
5. Pang, S. C.; Anderson, M. A.; Chapman, T. W. J Electrochem Soc 2000, 147, 444.
6. Reddy, R. N.; Reddy, R. G. J Power Sources 2004, 132, 315.
7. Toupin, M.; Brousse, T.; Belanger, D. Chem Mater 2004, 16, 3184.
8. Subramanian, V.; Zhu, H.; Vajtai, R.; Ajayan, P. M.; Wei, B. J Phys Chem B 2005, 109, 20207.
9. Chaudhary, Y. S.; Agrawal, A.; Shrivastav, R.; Satsangi, V. R.; Dass, S. Int J Hydrogen Energy 2004, 29, 131.
10. Yoon, K. H.; Choi, W. J.; Kang, D. H. Thin Solid Films 2000, 372, 250.
11. Maity, A.; Biswas, M. J Appl Polym Sci 2004, 94, 803.
12. Yang, Q. B.; Li, D. M.; Hong, Y. L.; Li, Z. Y.; Wang, C.; Qiu, S. L.; Wei, Y. Synth Met 2003, 137, 973.
13. Yang, X.; Shao, C.; Liu, Y.; Mu, R.; Guan, H. Thin Solid Films 2005, 478, 228.
14. Lee, S. W.; Kim, Y. U.; Choi, S. S.; Park, T. Y.; Joo, Y. L.; Lee, S. G. Mater Lett 2006, 61, 889.
15. Bailar, J. C.; Emeleus, H. J.; Nyholm, R.; Trotman-Dickenson, A. F. Comprehensive Inorganic Chemistry; Pergamon Press: New York, 1973.
16. Xi, J.; Tang, X. Chem Phys Lett 2004, 393, 271.
17. Xi, J.; Qiu, X.; Zhu, W.; Tang, X. Microporous Mesoporous Mater 2006, 88, 1.
18. Pereira, R. P.; Rocco, A. M.; Bielschowsky, C. E. J Phys Chem B 2004, 108, 12677.
19. Kayan, A.; Tarcan, E.; Kadiroglu, U.; Esmer, K. Mater Lett 2004, 58, 2170.